Int. J. Heat Mass Transfer. Vol. 30, No. 8, pp. 1645–1654, 1987
Printed in Great Britain

0017-9310/87 $3.00+0.00

Mixed convection between horizontal plates—I. Entrance effects

KUAN-CHENG CHIU† and FRANZ ROSENBERGER†
Department of Physics, University of Utah, Salt Lake City, UT 84112, U.S.A.

(*Received* 16 *June* 1986 *and in final form* 28 *January* 1987)

Abstract—Entrance effects in mixed convection between horizontal, differentially heated plates were studied in nitrogen by laser Doppler anemometry in a range $1368 < Ra < 8300$ and $15 < Re < 170$. Two entrance lengths were deduced from velocity profiles: one for the onset of buoyancy-driven convective instability, and one for the full development of the mixed flow. Explicit expressions for both entrance lengths are given. In addition, unsteady longitudinal convection rolls were observed. These are discussed in terms of an admixture of transverse convection rolls and/or contributions from upstream turbulence. The experimental results show that the critical Ra for the transverse convection rolls increases as Re increases.

1. INTRODUCTION

INVESTIGATIONS of the fluid dynamics of chemical vapor deposition (CVD) of solid layers [1–8] or of the cooling of electronic equipment [9, 10] underscore questions about entrance effects in mixed convection. In these systems, buoyancy-induced flow modulates the forced flow, leading to complicated, three-dimensional (3-D), mixed convection. Further complications arise from the strong temperature dependence of the properties of gases. Hence, the entrance length for purely forced convection (i.e. without buoyancy and for constant properties), though often quoted in the CVD literature, can shed little insight on the real conditions in these systems.

In this paper, as a precursor to a study of the flow in laterally bound CVD reactors, we focus on the entrance effects of mixed convection in a channel formed by two horizontal, parallel plates, which are isothermally heated from below and cooled from above. Even for this case, analytical solutions are intractable and 3-D numerical schemes are not well developed as yet. Various approximations have been made. For example, the fully developed flow assumption reduces the 3-D to 2-D problems [3, 10, 11]. However, it is still important to know in which region of the channel this simplification can be applied.

Due to the temperature dependence of the properties and, for supercritical conditions, due to the modulation caused by the buoyancy-induced flow, the energy and momentum equations are strongly coupled. The development of the temperature profile is closely linked to the development of the velocity profiles. Therefore, it is not necessary to distinguish between the thermal and hydrodynamic entrance lengths. Instead, according to the flow behavior as schematically indicated in Fig. 1, we will introduce two terms, namely, the entrance length for the onset of buoyancy-driven convective instability, L_1, and the entrance length for the full development of the mixed flow, L_2. The channel can then be divided into three regions: a region dominated by forced flow ($0 < x < L_1$), a transition region ($L_1 < x < L_2$), and a fully developed mixed flow region ($x > L_2$).

The L_1 for longitudinal convection rolls (with axes parallel to the forced flow direction) can be deduced from earlier studies [12–14] of $Ra_{cr}(x, Re)$, i.e. from the $Ra(Re)$ required at a given downstream x for the onset of buoyancy-driven instability. Hwang and Cheng [12] used linear stability theory, based on the Boussinesq approximation, to predict $Ra_{cr}(x, Re)$ for select Res. Kamotani and Ostrach [13] observed from temperature profiles that the experimental values of Ra_{cr} are about two orders of magnitude larger than theoretically predicted [12]. Later Hwang and Liu [14] conducted flow visualization experiments and confirmed the finding of ref. [13]. Both theoretical [12] and experimental [14] works qualitatively show that L_1 depends nonlinearly on Re and Ra.

The L_2 for longitudinal convection rolls has not

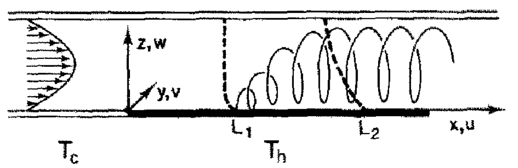

FIG. 1. Mixed convection flow between horizontal differentially heated plates for $Ra > Ra_c$. Dashed curves: schematic temperature profiles. L_1: entrance length for the onset of buoyancy-driven convective instability, L_2: entrance length for the full development of longitudinal rolls.

† Now at Center for Microgravity and Materials Research, University of Alabama in Huntsville, Huntsville, AL 35899, U.S.A.

NOMENCLATURE

f_D	Doppler frequency, $2u \sin\alpha/\lambda$
Δf_D	half-amplitude bandwidth of Doppler signal from spectrum analyzer
g	gravitational acceleration, 980 cm s^{-2}
Gr	Grashof number, Ra/Pr
H	height of the channel, 1.58 cm
L_1	entrance length for the onset of buoyancy-driven convective instability, experimental results for AR = 10, equation (1)
L_2	entrance length for the full development of the mixed flow, experimental results for AR = 10, equation (2)
P_0	mean pressure
Pr	Prandtl number, ν/κ
Ra	Rayleigh number, $\beta g \Delta T H^3/\nu\kappa$
Ra_c	critical Ra for Rayleigh–Benard convection, 1708
$Ra_{c,t}$	critical Ra for the transverse convection rolls
Ra_{cr}	condition marking the onset of instability at a given x and Re, same notation as used in ref. [12]
Re	Reynolds number, $u_0 H/\nu$
T_0	average temperature, $(T_h + T_c)/2$
T_c	temperature of the cold plate and isothermal section
T_h	temperature of the hot plate
ΔT	$T_h - T_c$
u, v, w	velocity components in the x-, y- and z-direction
u_0	average velocity, $u_{max}/1.5$, to simulate the laterally unbound configuration
u_{max}	maximum u-velocity at $x = -3H$
Δu	modulation amplitude of u-velocity at $z = H/2$ in fully developed region
W	width of the channel, 15.24 cm
x, y, z	Cartesian coordinates.

Greek symbols

α	half angle between two laser beams
β	thermal expansion coefficient [K^{-1}]
ε	reduced Rayleigh number, $(Ra - Ra_c)/Ra_c$
κ	thermal diffusivity [cm^2 s^{-1}]
λ	wavelength of laser
ν	kinematic viscosity [cm^2 s^{-1}]
ρ	density of gas [g cm^{-3}].

Abbreviations

2-D	two-dimensional
3-D	three-dimensional
AR	aspect ratio = width/height
LDA	laser Doppler anemometry.

been theoretically treated as yet. Experimental works by Kamotani and co-workers [13, 15] gave some preliminary results. In their first paper [13], they concluded from vertical temperature profiles at $Ra = 1000$ and $Ra = 31\,000$ that the thermal entrance length for a range $1000 < Ra < 31\,000$ is almost independent of Ra and the same as that for subcritical Ras. Later [15], they found that for a range $22\,000 < Ra < 210\,000$ the thermal entrance length depends on Re^2/Gr.

In this paper, we will present explicit expressions for L_1 and L_2 in the region $1368 < Ra < 8300$ and $15 < Re < 170$. The entrance lengths will be deduced from velocity profiles measured by laser Doppler anemometry (LDA). In addition, unsteady longitudinal convection rolls were observed under two conditions: either for flows with combinations of low Re and high Ra or for flows without an isothermal entrance section. These will be discussed in terms of an admixture of transverse convection rolls (with axes perpendicular to the forced flow direction) and/or contributions from upstream turbulence.

2. EXPERIMENTAL APPARATUS AND TECHNIQUE

Figure 2 shows a schematic cross-section of the channel, and its support structure, used to simulate the laterally unbound mixed convection configuration discussed above. An aspect ratio (AR = W/H = width/height) of about 10 was chosen as a compromise between LDA viewing conditions and the simulation for the laterally unbound flow in the channel's mid-region. The channel was 15.24 cm wide and 1.58 cm high. The bottom and top were formed by 0.635 cm thick aluminum plates which were individually thermostated to temperatures T_h and T_c, respectively. The temperature uniformity obtained in these 87.5 cm long plates, as measured with thermistors as well as an infra-red thermometer, was $\pm 0.2^\circ$C for $\Delta T = 24^\circ$C. The sidewalls were made of 1.27 cm thick Plexiglas. In the upstream direction, this differentially heated test section was smoothly connected to an isothermal channel of the same cross-section, that was thermostated to T_c (Fig. 3). The length of this isothermal section of 63.5 cm was chosen such that all flows entering the test section with $Re < 170$ were hydrodynamically fully developed [16–19]. The bottom plates of the isothermal and test sections were thermally separated by a coplanar 0.32 cm wide Plexiglas strip. A reasonably parallel entrance flow into the isothermal section was achieved with a settling chamber that as schematically shown in Fig. 3 contained several flow-deflecting baffles. Exit effects in the test section were minimized by using a converging exhaust box. Both the settling chamber and exhaust

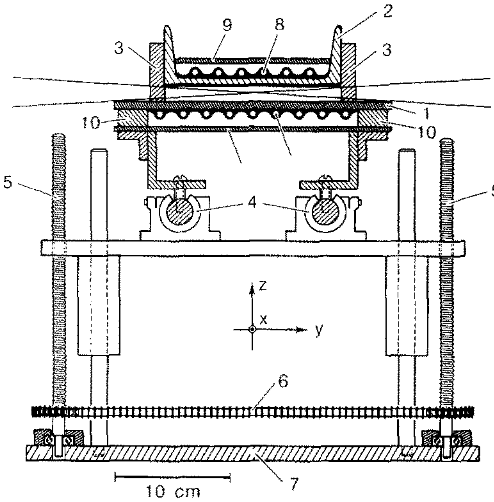

FIG. 2. Cross-section of the channel and three-dimensional translation table. (1) Bottom plate; (2) top plate beam; (3) sidewalls; (4) linear bearings for coarse x-translation; (5) four-spindle lift for z-translation (synchronized with timing belt (6)); (7) x–y translation milling table; (8) heating coils; (9) convection barriers (wood); (10) conduction barriers (Plexiglas).

box were made of Plexiglas, which facilitates the evaluation of their function with smoke-flow patterns.

As can be seen in Fig. 2, the whole channel was mounted on linear bearings (Thomson Inc. SPB-12-OPN) for coarse translation in the x-direction. The translation in the z-direction was facilitated by mounting the base of the x-translation bearings on a synchronized four-spindle lift which stood on a large milling table. The milling table had a y-translation arrangement and was also used for fine x-translation. This three-coordinate translation capability allowed us to position the stationary measuring spot of the laser anemometer throughout the channel.

As indicated in Fig. 3, the commercial LDA system (TSI Inc.) consisted of a He–Ne laser (15 mW), beam splitter and transmitting optics, collecting optics and photomultiplier (on axis), band-pass filter and a fast Fourier transform spectrum analyzer (Nicolet model 440B). The LDA measuring volume dimensions in the x- and y-direction were 0.2 and 2.1 mm, respectively. Seeds for light scattering were generated in a constant output atomizer (TSI model 3076) from an aqueous NaCl solution. In order to properly move with the flow, at the low flow velocities investigated, the seed size must not exceed a few tenths of a micron. This was obtained in the given atomizer under 35 psig of nitrogen with 0.2 g of NaCl per ml of water after diffusion drying of the aerosol during passage through a chamber lined with silica gel. Neutralization of the electrostatically charged particles was achieved in a radioactive neutralizer (TSI model 3012). The dry and neutral particles were then mixed with the volumetrically controlled main nitrogen flow and fed through the settling chamber into the channel.

Before the systematic studies of the flow dependence on *Ra* and *Re*, we ascertained that the hydrodynamically fully developed flow (at $x = 0$, the beginning of the test section) in the middle part of the channel (y around $0.5W$) is indeed 2-D. The $u(y, z)$ velocity profile for a hydrodynamically fully developed flow in a rectangular duct can be computed analytically [20]. The $u(y/W)$ profile is flat over the central 70% of the channel width for AR = 10 (80% for AR = 20). As shown in Fig. 4, our LDA results obtained at $x = 0$ agree well with the analytical solution.

The uncertainties in *Ra* and *Re*, resulting essentially from the uncertainties in channel height, surface temperature and limited steadiness of the forced flow, are estimated to not exceed 5%. The thermophysical parameters and operation conditions used for the computation of *Ra* and *Re* are listed in Table 1. The error bars shown in the velocity profiles represent

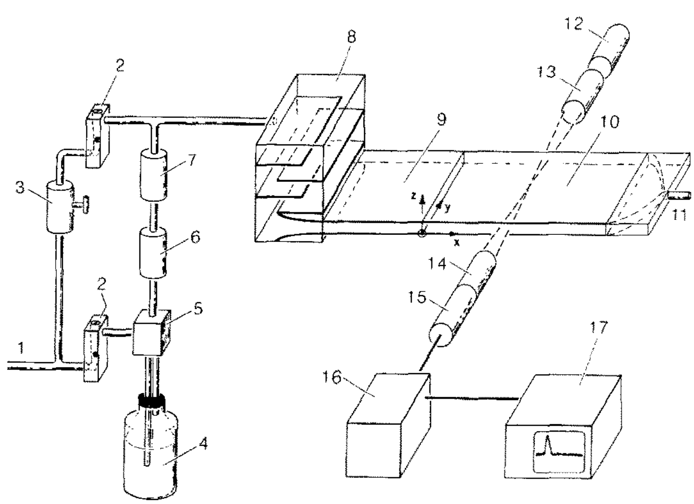

FIG. 3. Schematic diagram of experimental apparatus. (1) N_2 inlet (35 psig); (2) flow meters; (3) pressure regulator; (4) NaCl solution; (5) atomizer; (6) diffusion dryer; (7) neutralizer; (8) settling chamber; (9) isothermal entrance section; (10) test section; (11) exhaust; (12) laser; (13) transmitting optics; (14) collecting optics; (15) photomultiplier; (16) band-pass filter; (17) FFT spectrum analyzer.

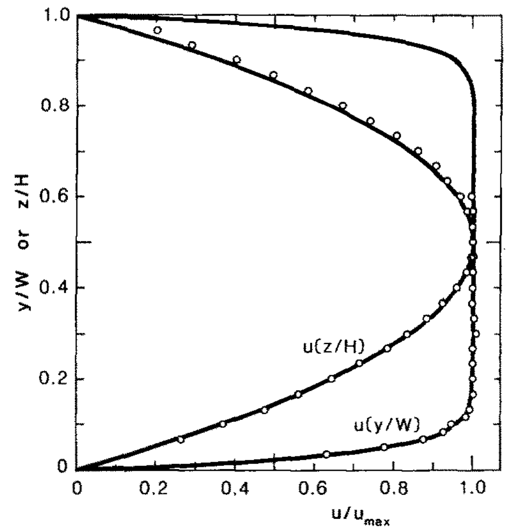

FIG. 4. Longitudinal velocities $u(y/W)$ at $z = 0.5H$ and $u(z/H)$ at $y = 0.5W$ for hydrodynamically fully developed flow with AR = 10. Circles: experimental data; solid curves: analytical solutions.

the half-amplitude bandwidth (Δf_D) of the Doppler signal (f_D) obtained from the spectrum analyzer. These bandwidths are mainly determined by the instrument resolution (finite number of fringes in measuring volume), the velocity gradients across the measuring volume, and some unsteadiness in the flow structure of the rolls. The large variations in error bars result mostly from the large changes in velocity gradients between adjacent measuring points at certain locations.

3. RESULTS AND DISCUSSION

3.1. *Entrance length for the onset of buoyancy-driven instability*

For the experimental determination of L_1, the $u(x, y)$ velocity profiles at $z = 0.2H$ were measured for various combinations of Ra and Re. Since the entering forced flow is heated from below, the buoyancy-driven instabilities occur first in the region close to the heated bottom plate, i.e. in the thermal boundary layer. Then the u-velocity is modulated by these instabilities due to the momentum coupling as is shown in the sequel to this paper [11]. Thus, the $u(x, y)$ velocity profiles at $z = 0.2H$ were chosen to detect the onset of instability. Figure 5 shows the results for $Ra = 4878$ and $Re = 44.8$. In order to compare our results to those for laterally unbound flow, we focus on the flow in the central region (y = 6–9 cm) of the channel. Effects from the sidewalls will be discussed in the next section.

The onset of instability is based on the following operational definition: when the change of the $u(y)$ velocity profile in the central region at $z = 0.2H$ exceeds 3% of $u(x = 0, y = 0.5W, z = 0.2H)$. Based on this definition, we see from the coarse measurement grid of Fig. 5 that L_1 lies between $10 < x < 20$ cm. In order to determine L_1 more precisely, $u(y)$-velocity profiles were measured with closer spacings throughout this range in x. The results, together with those for all other Re–Ra combinations investigated, are summarized in Table 2. A least square fit to these data yields

$$L_1 = (0.65 \pm 0.05) H \varepsilon^{-0.44 \pm 0.01} Re^{0.76 \pm 0.02} \quad (\varepsilon > 0) \tag{1}$$

where $\varepsilon = (Ra - Ra_c)/Ra_c$ represents the reduced Rayleigh number, and Ra_c represents the critical Ra for Rayleigh–Benard convection. The experimental data (with error bars) and fitted curves (heavy, with fields corresponding to the above standard deviations) for three Ras are shown in Fig. 6. A comparison of equation (1) and the theoretical predictions [12] shows that our experimental results are about 50 times larger. Yet our results are in agreement with other experimental findings [13, 14].

In order to explain the disagreement between the theoretical prediction and experimental results, Kamotani *et al.* [15] suggested that the thermal boundary layer thickness may be the proper vertical length scale of Ra_{cr}. However, Hwang and Cheng [12] had included the effect of the developing thermal boundary layer in the entrance region. This can be seen from Fig. 6 in ref. [12] where Ra_{cr} decreases with increasing x. We feel that the disagreement can be attributed to two factors: the difference between infinitesimal disturbances assumed in theory and measurable dis-

Table 1. Operation conditions for N_2 at $P_0 = 0.85$ atm

T_c (K)	T_h (K)	T_0 (K)	ν ($cm^2 s^{-1}$)	$g\beta/\nu^2$ ($cm^{-3} K^{-1}$)	$Pr = \nu/\kappa$	Ra
296.0	301.0	298.5	0.184	97.7	0.71	1368
296.0	305.4	300.7	0.186	93.9	0.71	2472
296.0	311.0	303.5	0.189	90.2	0.71	3789
296.0	316.0	306.0	0.192	87.1	0.71	4878
296.0	324.0	310.0	0.196	82.2	0.71	6446
296.0	335.0	315.5	0.202	76.0	0.71	8300

Note:
(1) P_0 is the pressure measured at the inlet of the isothermal section.
(2) Only the density has been corrected, through the ideal gas law, at $P_0 = 0.85$ atm.
(3) The physical properties are based on T_0 and calculated from ref. [28].

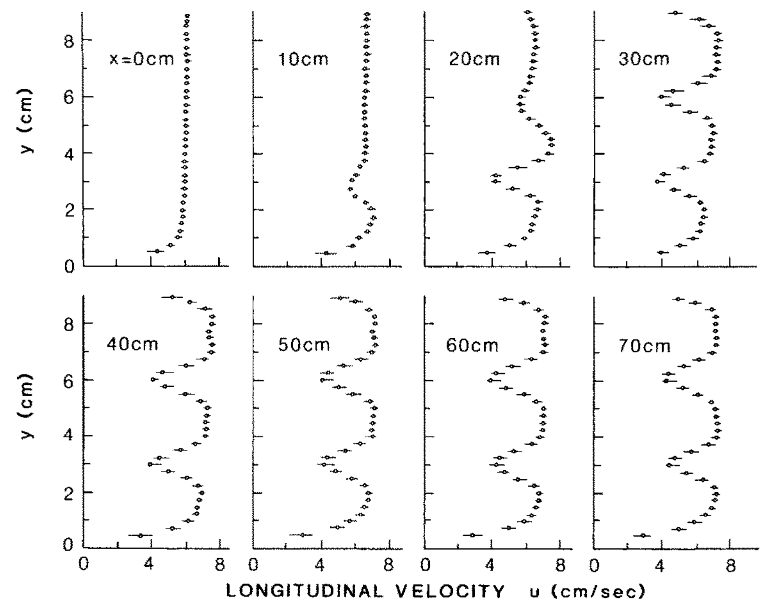

FIG. 5. Longitudinal velocity profiles $u(y)$ measured at $z = 0.2H$ and different x-positions for $Re = 44.8$ and $Ra = 4878$.

Table 2. Experimental values for L_1

Ra	Re	L_1 (cm)
2472	18.1	15–16
	32.5	20–22
	52.8	26–28
	74.3	32–34
3789	17.7	9–10
	31.8	12–13
	53.8	19–21
	74.5	25–30
	102.2	38–42
	129.4	43–45
4878	31.6	9–11
	71.7	20–22
	127.3	33–37
	170.8	40–50
6446	101.1	25–27
	127.3	32–35
8300	68.3	10–12
	95.5	15–16
	120.2	18–20
	161.8	24–30

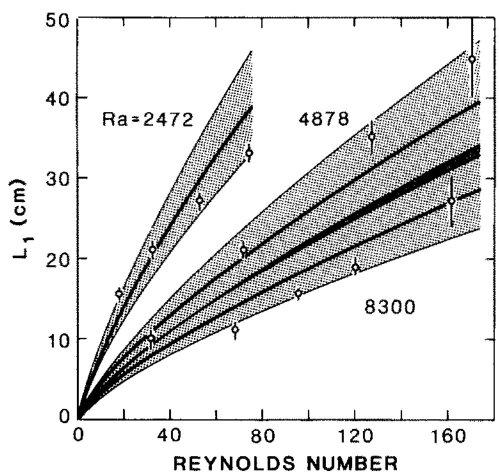

FIG. 6. Entrance lengths L_1, experimental data and least-square curves (see text).

turbances required for experiment [21], and the slow development of the spontaneous fluctuations near the critical state [22]. This 'critical slowing down' leads to a longer growth time and, hence, larger L_1 required for the entrained infinitesimal disturbances to become observable.

3.2. *Entrance length for the full development of the mixed flow*

In this section we will consider only fully developed, steady, longitudinal convection rolls. The conditions required to reach this steady flow will be discussed in the next section.

For the experimental determination of L_2, the same procedure was followed as that for the measurement of L_1, except the $u(x, y)$ velocity profiles were measured at $z = 0.5H$. As shown in Fig. 7, the shape of the $u(y)$ velocity profiles remains practically constant (i.e. the flow is fully developed) after a certain axial distance. Hence, we chose the modulation amplitude of $u(y)$ velocity profile in the fully developed region, Δu, as a criterion and used the following operational definition: the flow is called fully developed when the modulation amplitude of the $u(y)$ velocity profiles at $z = 0.5H$ in the central region (y = 6–9 cm) of the channel reaches 95% of Δu. Based on this definition, we see from the coarse measurement grid of Fig. 7 that, for $Ra = 4878$ and $Re = 44.8$, the full development of the longitudinal convection rolls is reached

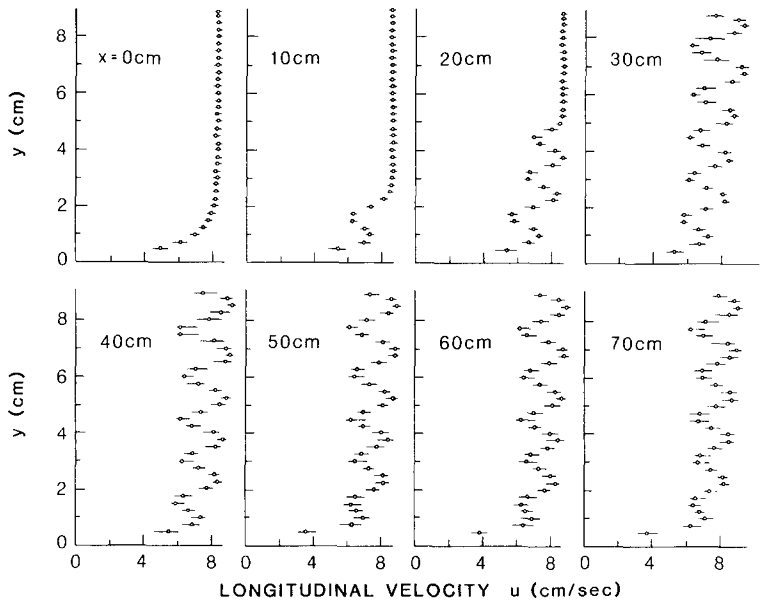

FIG. 7. Longitudinal velocity profiles $u(y)$ measured at $z = 0.5H$ and different x-positions, for $Re = 44.8$ and $Ra = 4878$.

Table 3. Experimental values for L_2

Ra	Re	L_2 (cm)
2472	17.8	30–32
	32.5	50–55
3789	17.7	13–15
	31.8	23–25
	53.3	39–42
4878	31.6	16–20
	44.8	26–29
	52.8	32–35
	71.7	40–45
6446	45.5	20–22
	53.0	23–25
	70.8	30–33
	100.6	42–45
8300	53.4	18–20
	71.7	25–27
	120.2	41–43

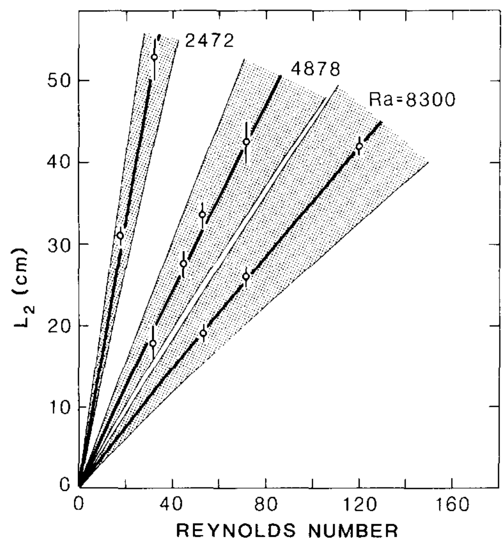

FIG. 8. Entrance lengths L_2, experimental data and least-square curves (see text).

between $20 < x < 30$ cm. The results with closer spacings in the x-direction and other combinations of Re–Ra are summarized in Table 3. A least-square fit to those data yields

$$L_2 = (0.68 \pm 0.07) H \varepsilon^{-0.69 \pm 0.02} Re^{0.96 \pm 0.03} \quad (\varepsilon > 0). \tag{2}$$

The experimental data (with error bars) and fitted curves (heavy, with fields corresponding to the above standard deviations) for three Ras are shown in Fig. 8. Our results clearly show, that in the region $2472 < Ra < 8300$, L_2 depends on Ra and Re. This is in contrast to earlier claims [13] which were deduced from a comparison of results for $Ra = 30\,000$ with those of subcritical flow and, hence, possibly missed the variation in the range between.

From Figs. 5 and 7 one sees that the buoyancy-induced flow first occurs near the sidewalls. Since the gases entering the channel (at $x = 0$) are essentially at $T = T_c$, the new thermal boundary condition at the sidewalls will always introduce temperature gradients. This horizontal temperature gradient will induce buoyancy-driven flow without threshold. In fact, the sidewalls can be regarded as sources for finite amplitude perturbations to the flow in the central region.

It is important to note that in the entrance region of a channel with small AR, say AR = 2 (typical of horizontal CVD reactors), the rolls induced by sidewalls will fill the whole channel even at subcritical Ras [1, 3, 4, 7]. For a channel with high AR and at

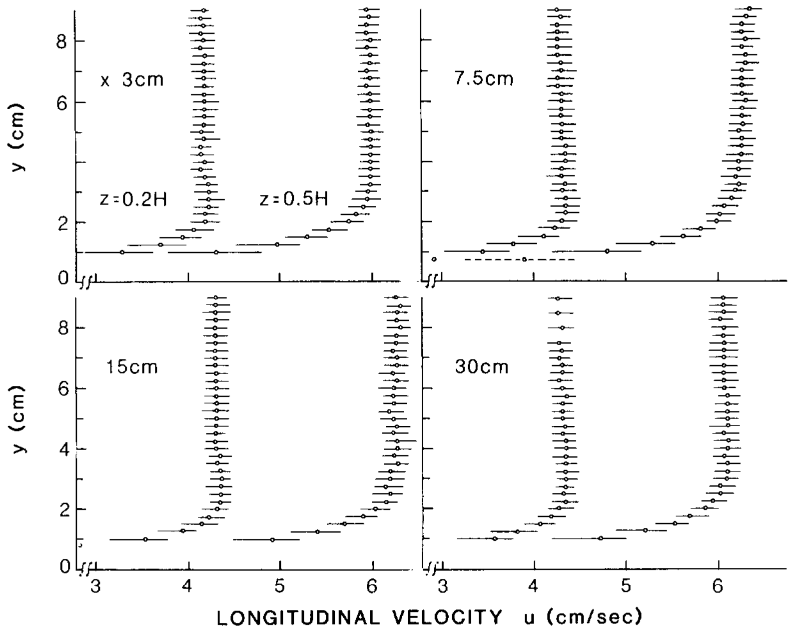

FIG. 9. Longitudinal velocity profiles $u(y)$ measured at $z = 0.2H$ and $0.5H$ and different x-positions for $Re = 30$ and $Ra = 1368$.

subcritical *Ra*s, as shown in Fig. 9 for AR = 10 and $Ra = 1368$, only the flow in the entrance region and near the sidewall is perturbed, while the flow in the central region remains essentially unchanged. Hence, this flow can be considered as a 2-D forced convection flow. The increase in u-velocity of about 5% in the x-direction (as shown in Fig. 9) can be accounted for by the thermal expansion of the gas and uncertainties in the measuring position of z. This sidewall effect for high AR channels at subcritical *Ra*s is in agreement with the findings by Wesfreid *et al.* [23]. These workers studied the influence of velocity perturbations imposed on sidewalls in a Rayleigh–Benard system (i.e. without forced flow). They found that the induced rolls were spatially damped exponentially with increasing distance from the wall. For supercritical *Ra*s, the effect of sidewalls on L_1 and L_2 depends on the AR of the channel. In general one will expect that both L_1 and L_2 decrease with decreasing AR. However, how much our results for AR = 10 deviate from those for laterally unbound flow remains to be investigated.

3.3. *Unsteadiness of the longitudinal convection rolls*

When unsteady flows are studied with LDA using a signal averaging time (45 s for our experiments) that is large as compared to the characteristic time of the velocity fluctuations, a widened half-amplitude bandwidth, Δf_D, results, which corresponds to twice Δu. This is reflected by the larger 'error bars' in u-velocity (e.g. Fig. 10(a)) as compared to those observed in steady flows (e.g. Fig. 10(b)).

With a simple flow visualization technique (light cuts in the y–z plane) the unsteady flow modes were identified as 'snaking' modulations of the longitudinal

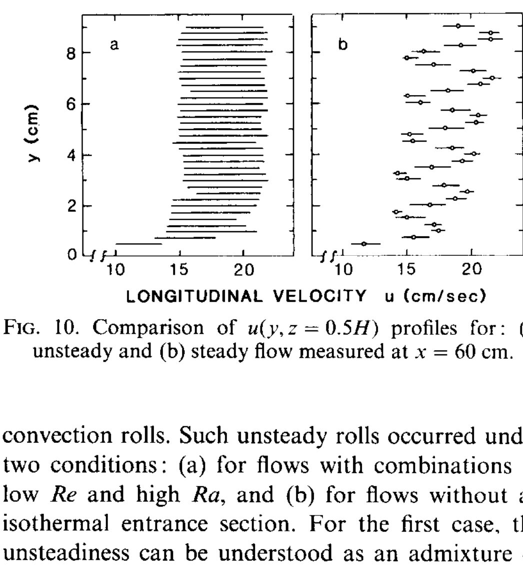

FIG. 10. Comparison of $u(y, z = 0.5H)$ profiles for: (a) unsteady and (b) steady flow measured at $x = 60$ cm.

convection rolls. Such unsteady rolls occurred under two conditions: (a) for flows with combinations of low *Re* and high *Ra*, and (b) for flows without an isothermal entrance section. For the first case, the unsteadiness can be understood as an admixture of transverse convection rolls. For the second case, the unsteadiness may come from contributions of upstream turbulence. Both aspects will be discussed in the following sections.

3.3.1. *Admixture of transverse convection rolls.* When an externally forced laminar flow is superimposed on the buoyancy-driven flow between two horizontal differentially heated plates, the critical *Ra* for the transverse convection rolls, $Ra_{c,t}$, increases with *Re* [24–26]. But, as we have shown in ref. [11], the critical *Ra* for the longitudinal convection rolls is independent of *Re* and is equal to Ra_c. Therefore, when *Re* and *Ra* are such that $Ra_{c,t}(Re) > Ra > Ra_c$, only longitudinal convection rolls will exist. However, with combinations of *Re* and *Ra* such that $Ra > Ra_{c,t}(Re) > Ra_c$, transverse convection rolls will exist

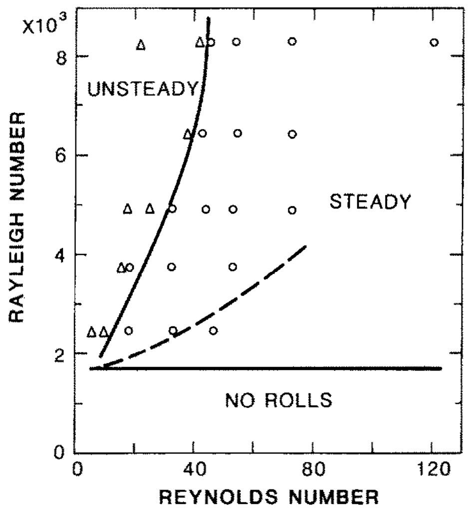

FIG. 11. Regimes for fully developed longitudinal convection rolls.

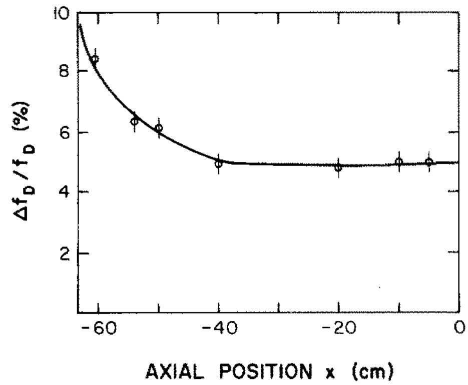

FIG. 12. Variation of the normalized half-amplitude bandwidth within the isothermal entrance section (from $x = -63.5$ cm to $x = 0$).

in addition to the longitudinal convection rolls. Their combination with the forced flow results in a 'snaking' motion, i.e. time-dependent flow. Thus, from the onset of the unsteady longitudinal convection rolls, one can determine $Ra_{c,t}(Re)$.

Our experimental results for combinations of *Ra* and *Re* leading to steady and unsteady flow, respectively, are shown in Fig. 11 by circles and triangles. The characteristic (solid) curve separates these two regimes. The experimental error for this curve in terms of *Re* is estimated to be about 15%. The theoretical results based on the Boussinesq approximation and constant physical properties for $Pr = 0.7$ [25] are represented by the dashed curve in Fig. 11. Our experimental results of $Ra_{c,t}(Re)$ follow the same trend but lie considerably above the theoretical prediction. Again, this can possibly be attributed to the difference between infinitesimal disturbances in theory and finite amplitudes required for detection in an experiment [21].

3.3.2. *Contribution from upstream turbulence.* In the previous discussion we have assumed that the flows with low *Re*s entering the test section are laminar and possess a very low turbulence intensity (for definition of turbulence intensity see ref. [27]). These conditions were experimentally approximated with the long isothermal entrance section upstream from the test section (see Section 2). Thus, as we will see below, upstream turbulence, which is likely created in the sudden expansion of the narrow gas line into the settling chamber or during the flow through the baffles, was sufficiently damped out before the flow reached the test section. However, without this additional isothermal entrance section, some of the previously steady longitudinal rolls (especially at higher *Re*) became unsteady. As shown in Fig. 10, two velocity profiles (unsteady vs steady) were measured at the same axial position ($x = 60$ cm) and for the same *Ra* and *Re*. Figure 10(b) was obtained with an isothermal entrance section upstream from the test section. For Fig. 10(a), the bottom plate of the entrance section was also heated to T_h. Thus, the isothermal entrance section was eliminated and the upstream turbulence apparently less damped.

To study the turbulence intensity within the isothermal entrance section, the half-amplitude bandwidth of the Doppler signal (Δf_D), normalized by the Doppler frequency (f_D in the u-velocity), was measured along the x-direction at $y = 0.5W$ and $z = 0.5H$. As shown by Fig. 12, the normalized bandwidth ($\Delta f_D / f_D$) decays along the x-direction and approaches a constant value of about 5% after $x = -40$ cm (for a flow with $u_0 = 18$ cm s^{-1}). The constant is solely due to the instrument resolution, and the velocity gradient (along the z-direction) across the measuring volume. For the higher values of $\Delta f_D / f_D$, in order to ascertain that they are not due to the velocity gradient in the y-direction, the corresponding $u(y)$ profiles were measured. This showed that the velocity gradient in the y-direction in the central region ($y \sim 0.5W$) is negligible even as close to the settling chamber as $x = -60.5$ cm. Thus, we can conclude that the increase of $\Delta f_D / f_D$ in Fig. 12 is a measure of the turbulence intensity. If one assumes that the turbulence intensity is negligible at the end of the isothermal entrance section, the turbulence intensity at the beginning of the isothermal entrance section is estimated to be about 2–3% (i.e. half of the difference of $\Delta f_D / f_D$ between the beginning and the end, see Fig. 12).

The effect of upstream turbulence on laminar boundary layer flows was discussed by Schlichting [27]. He pointed out that an increase in the upstream turbulence produces two effects. First, it causes earlier transition to turbulence in the boundary layer. Second, a turbulence intensity of about 2.5% produces an increase in the local heat flux by about 80%. As shown in Fig. 10, we observed a third effect. The heating from below for a channel flow with a certain degree of turbulence intensity can cause the longitudinal convection rolls to become unsteady.

Similar phenomena, as reflected in convective temperature oscillations [2, 4] or unstable fringe patterns [7], were found in CVD reactors. Entrance flows in CVD reactors typically emanate from narrow gas lines and without an isothermal entrance section. Hence, they will always possess a relatively high degree of upstream turbulence intensity, which can be responsible for the observed unstedy flow patterns.

4. SUMMARY

From a study of entrance effects of mixed convection between horizontal plates in the range $1368 < Ra < 8300$ and $15 < Re < 170$, the following results were obtained.

(1) For $Ra > Ra_c$, the entrance lengths for the onset of buoyancy-driven instability and for the full development of the longitudinal convection rolls depend on Ra and Re. The explicit expressions derived from the experimental results for AR = 10 are given in equations (1) and (2).

(2) For the onset of buoyancy-driven instability, our results are about two orders of magnitude larger than theoretical predictions. However, this is in an agreement with other experimental works.

(3) For $Ra < Ra_c$, the flow in the central region for a channel with high AR can be regarded as a 2-D forced convection flow. For channels with small AR (typical of horizontal CVD reactors), the sidewall effects play an important role in the overall flow pattern.

(4) As shown in Fig. 11, the longitudinal convection rolls are unsteady due to an admixture of transverse convection rolls. The experimental results show that $Ra_{c,t}$ increases as Re increases. This agrees qualitatively with the theoretical predictions.

(5) A low degree of upstream turbulence at the beginning of the bottom heated section is essential for the steadiness of the longitudinal convection rolls.

Acknowledgements—Support of this work by the Ceramics and Electronic Materials Program of the National Science Foundation under Grant DMR-8408398 is gratefully acknowledged. Helpful discussions with Jalil Ouazzani, Tom Nyce and Mike Banish are very much appreciated.

REFERENCES

1. F. C. Eversteyn, P. J. W. Severin, C. H. J. v.d. Brekel and H. L. Peek, A stagnant layer model for the epitaxial growth of silicon from silane in a horizontal reactor, *J. Electrochem. Soc.* **117,** 925–931 (1970).
2. B. J. Curtis and J. P. Dismukes, Effects of natural and forced convection in vapor phase growth system, *J. Crystal Growth* **17,** 128–140 (1972).
3. R. Takahashi, Y. Koga and K. Sugawara, Gas flow pattern and mass transfer analysis in a horizontal flow reactor for chemical vapor deposition, *J. Electrochem. Soc.* **119,** 1406–1412 (1972).
4. V. S. Ban, Transport phenomena measurements in epitaxial reactors, *J. Electrochem. Soc.* **125,** 317–320 (1978).
5. F. Rosenberger, Fluid dynamics in crystal growth from vapors, *PhysicoChem. Hydrodyn.* **1,** 3–26 (1980).
6. B. J. Curtis, Convective effects in open-tube chemical vapor deposition, *PhysicoChem. Hydrodyn.* **2,** 357–366 (1981).
7. L. J. Giling, Gas flow patterns in horizontal epitaxial reactor cells observed by interference holography, *J. Electrochem. Soc.* **129,** 634–644 (1982).
8. G. H. Westphal, Convective transport in vapor growth systems, *J. Crystal Growth* **65,** 105–123 (1983).
9. K. J. Kennedy and A. Zebib, Combined free and forced convection between horizontal parallel planes: some case studies, *Int. J. Heat Mass Transfer* **26,** 471–474 (1983).
10. M. E. Braaten and S. V. Patankar, Analysis of laminar mixed convection in shrouded arrays of heated rectangular blocks, *Int. J. Heat Mass Transfer* **28,** 1699–1709 (1985).
11. K.-C. Chiu, J. Ouazzani and F. Rosenberger, Mixed convection between horizontal plates—II. Fully developed flow, *Int. J. Heat Mass Transfer* **30,** 1655–1662 (1987).
12. G. J. Hwang and K. C. Cheng, Convective instability in thermal entrance region of a horizontal parallel-plate channel heated from below, *J. Heat Transfer* **95,** 72–77 (1973).
13. Y. Kamotani and S. Ostrach, Effect of thermal instability on thermally developing laminar channel flow, *J. Heat Transfer* **98,** 62–66 (1976).
14. G. J. Hwang and C. L. Liu, An experimental study of convective instability in the thermal entrance region of a horizontal parallel-plate channel heated from below, *Can. J. Chem. Engng* **54,** 521–525 (1976).
15. Y. Kamotani, S. Ostrach and H. Miao, Convective heat transfer augmentation in thermal entrance regions by means of thermal instability, *J. Heat Transfer* **101,** 222–226 (1979).
16. H. Schlichting, *Boundary Layer Theory*, 7th Edn, p. 186. McGraw-Hill, New York (1979).
17. H. Morihara and R. T.-S. Cheng, Numerical solution of the viscous flow in the entrance region of parallel plates, *J. Comput. Phys.* **11,** 550–572 (1973).
18. S. T. McComas, Hydrodynamics entrance lengths for ducts of arbitrary cross section, *J. Basic Engng* **89,** 847–850 (1967).
19. G. S. Beavers, E. M. Sparrow and R. A. Magnuson, Experiments on hydrodynamically developing flow in rectangular ducts of arbitrary aspect ratio, *Int. J. Heat Mass Transfer* **13,** 689–702 (1970).
20. R. K. Shah and A. L. London, *Laminar Flow Forced Convection in Ducts*, p. 197. Academic Press, New York (1978).
21. K. C. Cheng and R.-S. Wu, Axial heat conduction effects on thermal instability of horizontal plane Poiseuille flow heated from below, *J. Heat Transfer* **98,** 564–569 (1976).
22. P. Berge and M. Dubois, Rayleigh–Benard convection, *Contemp. Phys.* **25,** 535–582 (1984).
23. J. Wesfreid, P. Berge and M. Dubois, Induced pretransitional Rayleigh–Benard convection, *Phys. Rev.* **A19,** 1231–1233 (1979).
24. C. Klapisz, M. E. Weill and J. Chanu, Stability of laminar flow of a liquid mixture with temperature gradient, *Physica* **66,** 581–592 (1973).
25. J. K. Platten, A variational formulation for the stability of flows with temperature gradient, *Int. J. Engng Sci.* **9,** 855–869 (1971).
26. D. A. Nield, A note on the stability of laminar flow of a liquid mixture with temperature gradient, *Physica* **74,** 607–610 (1974).
27. H. Schlichting, *Boundary Layer Theory*, 7th Edn, p. 313. McGraw-Hill, New York (1979).
28. W. M. Kays and M. E. Crawford, *Convective Heat and Mass Transfer*, 2nd Edn, p. 389. McGraw-Hill, New York (1980).

CONVECTION MIXTE ENTRE PLAQUES HORIZONTALES—I. EFFET D'ENTREE

Résumé—Des effets d'entrée en convection mixte entre des plaques horizontales, différemment chauffées sont étudiés dans l'azote par l'anémomètrie laser Doppler dans un domaine $1368 < Ra < 8300$ et $15 < Re < 170$. Deux longueurs d'entrée sont déduites des profils de vitesse: une pour l'apparition d'instabilité convective conduite par la gravité, et une autre pour l'établissement complet de l'écoulement mixte. Des expressions explicites pour les deux longueurs d'entrée sont données. On observe aussi des rouleaux de convection longitudinaux instables. Ils sont discutés à travers des rouleaux de convection transverses et pour les contributions de turbulence en amont. Les résultats expérimentaux montrent que le Ra critique pour les rouleaux de convection transverses augment lorsque Re croît.

MISCHKONVEKTION ZWISCHEN HORIZONTALEN PLATTEN—I. EINLAUFEFFEKTE

Zusammenfassung—Einlaufeffekte bei der Mischkonvektion zwischen horizontalen, unterschiedlich beheizten Platten wurden mit einem Laser-Doppler-Anemometer für Stickstoff in einem Bereich von $1368 < Ra < 8300$ und $15 < Re < 170$ untersucht. Zwei Einlauflängen wurden aus den Geschwindigkeitsprofilen abgeleitet: eine für das Einsetzen der auftriebsgesteuerten Instabilität und eine für die volle Ausbildung der Mischströmung. Für beide Einlauflängen werden explizite Ausdrücke angegeben. Außerdem werden instationäre längsgerichtete Konvektionswalzen beobachtet. Diese werden als Beimischung von quergerichteten Konvektionswalzen und/oder als Beiträge der stromaufwärts vorhandenen Turbulenz diskutiert. Die experimentellen Ergebnisse zeigen, daß die kritische Ra-Zahl für die quergerichteten Konvektionswalzen mit der Re-Zahl ansteigt.

СМЕШАННАЯ КОНВЕКЦИЯ МЕЖДУ ГОРИЗОНТАЛЬНЫМИ ПЛАСТИНАМИ—I. НАЧАЛЬНЫЙ УЧАСТОК

Аннотация—Изучался начальный участок при смешанной конвекции между горизонтальными различно нагреваемыми пластинами с помощью метода лазерной допплеровской анемометрии при $1368 < Ra < 8300$ и $15 < Re < 170$. Различались два начальных участка: начала конвективной неустойчивости, вызванной подъемной силой и полного развития смешанного течения. Приведены выражения в явном виде для длин обоих участков. Кроме того, наблюдались нестационарные продольные конвективные валы. Обсуждена возможность их появления за счет перемешивания конвективных валов и/или вклада турбулентности от восходящего течения. Экспериментальные результаты показывают, что критическое Ra для поперечных конвективных валов увеличивается с ростом Re.